Systematic uncertainties of atomic data in photoionization modeling

Ballhausen, R.; Kallman, T.R.; Gu, Y.; Paerels, F.

CrossMark

Systematic Uncertainties of Atomic Data in Photoionization Modeling

R. Ballhausen[1,2] , T. R. Kallman[2] , L. Gu[3,4,5] , and F. Paerels[6]

[1] University of Maryland, Department of Astronomy, College Park, MD 20742, USA; ballhaus@umd.edu
[2] NASA Goddard Space Flight Center, Code 662, Greenbelt, MD 20771, USA
[3] SRON Netherlands Institute for Space Research, Niels Bohrweg 4, 2333 CA Leiden, The Netherlands
[4] RIKEN High Energy Astrophysics Laboratory, 2–1 Hirosawa, Wako, Saitama 351-0198, Japan
[5] Leiden Observatory, Leiden University, PO Box 9513, 2300 RA Leiden, The Netherlands
[6] Columbia University, New York, NY 10027, USA

Abstract

Fitting plasma models to high-quality spectra is a crucial tool for deriving diagnostics about the physical conditions in various astrophysical sources. Despite decades of model development, this prescription often provides an unsatisfying description of observational data. We explore some of the origins of the failure of fits of photoionized plasma models to high-resolution X-ray spectra. In particular, we test whether systematic uncertainties in underlying atomic data can account for data model discrepancies, and whether including model uncertainties during spectral fitting can provide statistically acceptable fits and reasonable parameter estimates. We fit Chandra/ HETG spectra of NGC 3783 with the photoionized absorber model `warmabs`. We use the remaining data model discrepancies to estimate the systematic uncertainties of bound–bound radiative rates for individual transitions quantitatively. We then include these uncertainties into `warmabs` to return a total model uncertainty. We find residual data model discrepancies which are due to systematic errors that cannot be accounted for solely by a modification of the optical depth of strong absorption lines. Furthermore, statistical uncertainties still dominate the fit statistics. The relevance of model uncertainties in spectral fitting will vary on a case-by-case basis. However, they are likely to have a minor effect on most of the currently existing data sets. We conclude that while the quality of atomic data does have an effect on fitting photoionization models, and so demands further improvement, uncertainties in radiative rates cannot be held solely responsible for statistically unacceptable fits. Other sources of systematic uncertainties are likely to be of comparable importance and require further investigation.

1. Introduction

We see signatures of ionized plasmas in spectra from all kinds of astrophysical objects. Fitting physical plasma models to high-quality spectral data is the key to understanding the properties of these plasmas as well as the sources which power them. Our conclusions about physical conditions in astrophysical X-ray sources therefore depend critically on the quality of physical plasma models. However, when reviewing the literature regarding the success of applying these models to observational data, two general outcomes frequently occur, each raising a number of follow-up questions.

If the model does not describe the data well, then it has to be rejected on statistical grounds. The most plausible conclusion then would be that the choice of the model was inappropriate for the physical properties of the source at hand (for example, photoionized versus collisionally ionized plasma models, reflected versus transmitted radiation, etc.) But the failure of alternative models, or the need to construct models so complex that it limits their interpretation, might also indicate more subtle issues.

On the other hand, if a final fit statistic very close to an expected value can be obtained, then it is tempting to interpret uncertainties quoted on model parameters as purely statistical.

If so, it is not clear to what extent systematic uncertainties introduced by model assumptions and atomic data contribute to the error budget of derived model parameters.

In either of these scenarios, it is not clear what is the most important factor affecting the fit statistic. Possibilities include: pure counting statistics; the accuracy of the instrument calibration used during the fitting; the comprehensiveness, accuracy, or physical appropriateness of the model; or other computational expedients used in the fitting procedure. Of these, counting statistics should be properly accounted for by the tests embodied in the values of the C or χ^2 statistics used by `xspec` (Arnaud 1996), `isis` (Houck & Denicola 2000), `SPEX` (Kaastra et al. 1996), or other fitting tools.

Calibration, as embodied in the Redistribution Matrix File (RMF) and Ancillary Response File files used in the fitting, should be accounted for using data obtained prior to launch, and from standard sources during flight. Calibration data includes effective area, energy scale, background, and corrections for scattering within the instrument. Corrections for background or non-sky sources of counts also fall under this category. Ground-based and in-flight calibration of satellite-borne instruments is an ongoing effort, and reliable cross calibration among different instruments is strongly promoted by the International Astronomical Consortium for High-Energy Calibration (IACHEC).[7] Including calibration uncertainties in the data analysis poses additional statistical challenges, and we refer to Drake et al. (2006), Lee et al. (2011), and Xu et al. (2014) for their

---

[7] https://iachec.org/about-iachec/

statistical treatment in a Bayesian framework. A review of challenges in treating systematic uncertainties in both Bayesian and frequentist approaches is given by Heinrich & Lyons (2007). Finally, we must acknowledge the possibility of contributions to the fit statistic which do not fit into any other category. A possible example is the use of "stacking" or the addition of data Pulse Height Amplitude files from different observations; this procedure will introduce unwanted counts in the resulting spectrum if the source varies between the different observations and if the instrumental background is significant.

In addition to these effects which impair the quality of the observational data, their interpretation may eventually be affected by model inaccuracies (here and in what follows reserve the term "errors" for quantitative error estimates) which can take various forms. In this work we focus on astrophysical plasma codes that are widely used for the interpretation of high-resolution spectral data and used to infer physical quantities such as elemental abundances, temperatures, and column or particle densities. These codes calculate the response of gas to irradiation by an X-ray source or heating to a specific temperature. The codes then calculate various quantities such as charge state distributions (CSD), level populations, heating and cooling rates, and line emissivities and opacities that eventually allow for the prediction of a model spectrum that can be compared with observational data.

Sources of uncertainties that may affect the final data products include the accuracy of individual numerical calculations (e.g., numerical integrations, solving differential equations, or discretization of continuous quantities) or inherent physical assumptions or simplifications. Examples of these include the neglect of time dependence, density gradients, etc., or assumptions about the source geometry (e.g., spherical symmetry of the gas cloud, homogeneity of the absorbing medium).

One particular source of systematic uncertainties in astrophysical plasma models is the underlying atomic data: line and edge energy values, atomic rate coefficients affecting the level populations and ion fractions, and values of oscillator strengths or equivalent affecting line and edge emissivities or opacities. Inaccurate transition energies might lead to misplaced lines in the final spectrum with consequences ranging from incorrect velocity shifts to complete mis- or non-identification of a spectral line. Uncertainties in transition probabilities on the other hand might translate into inaccurate level popoulations affecting several derived quantities such as temperatures, line opacities, or ionization parameters.

While significant effort has gone into understanding the behavior of most of the contributions to the fit statistic, understanding the accuracy of atomic data is both the most straightforward and also the most difficult, owing to the number of distinct transition energies, atomic rates, and cross sections needed for spectral models. Atomic databases for spectral modeling have attained considerable size and complexity since the advent of Chandra and XMM-Newton. The vast majority of atomic data come from theoretical calculations, and only a comparatively small subset have been confirmed or refined by laboratory experiments. Uncertainty estimates on individual transitions are typically based on the comparison of results of different atomic codes, and this may lead to values that are spuriously larger or smaller than they should be, since it is likely that not all codes deserve equal weight when determining the favored value or the dispersion in values. Detailed comparisons are not feasible to explore atomic

uncertainties across the entire likely parameter space. Furthermore, such comparisons may underestimate important uncertainties due to similar assumptions or computational techniques utilized in the various atomic calculations. Our current primitive understanding of the contribution of atomic data inaccuracies to spectral fitting makes it tempting to blame atomic data inaccuracies for imperfect spectral fits, and also makes it more difficult to confidently rule in or out specific physical scenarios for spectral models.

In fact, conclusions about the validity of model physical assumptions, or the need for alternative models, often comprise the chief scientific result obtained from spectral fitting. A prominent showcase of the importance of the quality of atomic data for astrophysical plasma models was the Hitomi observation of the Perseus Cluster Hitomi Collaboration et al. (2018), which revealed discrepancies in the results from different collisional equilibrium plasma codes.

Recent high-quality observations, most prominently the Hitomi observation of the Perseus cluster, have brought longstanding questions about the required accuracy of atomic data for astrophysical plasma models and the understanding of their systematic uncertainties into focus again. Exemplary studies of databases for collisional plasma codes have been presented by Foster & Heuer (2020), Foster (2020) and Heuer et al. (2021) for APEC with AtomDB and Gu et al. (2022) for SPEX/CIE.

In this work we attempt to better characterize the effects of atomic data uncertainties and their contributions to the fit statistics for high-quality X-ray spectra of photoionized sources. That is, we test the hypothesis that data model discrepancies are solely due to uncertainties in the underlying atomic data and that these can be quantified by comparison with high-quality observational data. Our procedure is to revisit archival high-quality data of the Seyfert I galaxy NGC 3783, which is well known for its photoionized absorber and exhibits a large number of absorption lines from various elements and ionization states. We fit those with the photoionization code xstar/warmabs. We discuss the statistical quality of the models, the accuracy of the atomic database, and the model's physical assumptions and their impact on derived parameters. We then assume that the observed spectrum can be used to find the true strengths of the absorption features in the photoionized spectrum, i.e., that the observed spectrum is a more accurate realization of a photoionized plasma than our model. We do this by introducing *ad hoc* Gaussian components to the strongest absorption lines to compensate exactly for the discrepancies between the xstar/warmabs model and the observed data. In doing this, we follow the procedure outlined by Gu et al. (2022). We discuss the resulting changes to the fit statistic and the implications for our understanding of our atomic model. We then also explore what happens to the fit statistic and the best-fitting parameter values when these new atomic data error estimates are included during the fitting procedure in a manner analogous to the inclusion of statistical errors on the observed counts.

2. Data Selection and Extraction

In order to derive model error estimates from observed data, we require that our baseline observed data set be both high spectral resolution and signal-to-noise, as we can only constrain model uncertainties if statistical and instrumental calibration uncertainties are small in comparison. To this end, we use five

Table 1
Log of Observations of NGC 3783 Taken in 2001

ObsID	Start time (MJD)	Exposure (ks)	MEG (10^3 cts)	HEG (10^3 cts)
2090	51964.78	165.7	89.1	49.6
2091	51967.39	168.9	89.8	50.5
2092	51978.02	165.5	97.7	53.2
2093	51999.15	166.1	159.1	81.9
2094	52086.42	166.2	115.4	63.2

Note. Count numbers include both orders $+1$ and -1. Observation IDs (ObsID).

Chandra/HETG observations of the Seyfert I galaxy NGC 3783 taken in 2001 February–June using the Chandra High Energy Transmission Grating (HETG), which accumulated a total exposure of ~830 ks. NGC 3783 has been studied extensively in past years and is well known for the presence of an ionized absorber that is often modeled with a multi-component (typically 1–5 components, e.g., Kaspi et al. 2001; Krongold et al. 2003; Netzer et al. 2003; Gonçalves et al. 2006; Fu et al. 2017; Mehdipour et al. 2017) warm absorber model. We caution that still be some uncertainty regarding the physical completeness of the baseline model. Chandra/HETG lacks the capability to detect low ionization components such as those identified by the Reflection Grating Spectrometer and Cosmic Origins Spectrograph in Mehdipour et al. (2017) and Mao et al. (2019). These particular components do not generate absorption lines in Chandra/HETG but may impact the transmission of the continuum. Since we do intend to interpret the ionization and continuum parameters, we can neglect this effect.

An observation log is given in Table 1. We use CIAO v.4.12 with CALDB v.4.9.5 for data reprocessing. We apply `tgdetect2` and `tg_create_mask` to improve the zeroth order location and extraction regions. We then create level 2 event files with `chandra_repo` and finally extract source and background spectra with `tgextract2` along with appropriate response files. We apply the "optimal binning" scheme of Kaastra & Bleeker (2016) along with C-statistic (Cash 1979). We use `isis` v.1.6.2 for spectral fitting. Here and in what follows, parameter uncertainties are given at the 90% confidence level unless otherwise noted. The wavelength range we consider is 2.5–31 Å for the Medium Energy Grating (MEG) and 1.25–15 Å for the High Energy Grating (HEG). We further exclude the region of the spectrum containing the Fe Unresolved Transition Array (UTA) at 15.5–17 Å (see, e.g., Behar et al. 2001, for details), since these features are associated with gas which is at a distinct ionization parameter, and since there is no experimental data available to constrain either the line wavelengths or their oscillator strengths and widths. We fit all positive and negative first-order spectra of the MEG and HEG jointly to avoid known issues with coadding spectra due to calibration uncertainties[8] as well as additional systematic effects in the case of source variability.

3. Model Setup

The photoionization model is the semianalytical `warmabs` model (version 2.41), which is derived from the `xstar` photoionization code (Kallman & Bautista 2001). In order to reduce computation costs, `warmabs` relies on precalculated ion population files and performs only the calculation of the final optical depths of lines and edges and the broadening of absorption lines. The underlying assumptions are: (i) moderate optical depths such that forward scattering is negligible; (ii) the neglect of emission, either scattered or thermal (except see below); and (iii) an incident spectral energy distribution (SED) close to the one used in the calculation of the ion population files. Assuming only moderate optical depth further implies the absence of a significant ionization gradient associated with optical depth effects. A description of the `xstar` database is given by Mendoza et al. (2021).

We recalculated population files with default parameters with `xstar` v.2.58 c. To further reduce model runtimes to a level that allows for the systematic exploration of the model behavior, we tabulate the `warmabs` output on an energy grid appropriate for the Chandra/HETG RMF. We set the `llinabs`[9] switch to 1 to also include transitions flagged regarding wavelength accuracy in the `xstar` database. Our tabulated model allows $\log \xi$, N_H, and all elemental abundances to vary to optimize the fit, but we keep the turbulent velocity[10] fixed at $150 \, \mathrm{km \, s^{-1}}$ as reported in Kaspi et al. (2000). Our baseline abundances are Wilms et al. (2000).

Our continuum model consists of a power law and blackbody component with galactic neutral absorption modeled using the `tbabs` model with Wilms et al. (2000) abundances and cross sections of Verner & Yakovlev (1995). We further include a galactic redshift of $z = 0.0097$, as well as a set of empirical emission lines, in particular Fe I Kα (6403.48 eV), O VIII Lyα (653.49 eV), O VII Heα (560.98 eV, 568.62 eV, 573.95 eV), Ne X Lyα (1021.50 eV), Ne IX Heα (904.93 eV, 915.28 eV, 922.02 eV) that are not accounted for by our photoionization model, since it only produces absorption features. We fix the width of these emission features according to the same turbulent velocity of the `warmabs` model and only fit the line flux. An interpretation of these fluxes is, however, beyond the scope of this paper. We allow the power-law photon index, blackbody temperature, and their respective normalizations to vary between individual observations to account for source intrinsic variability, as was reported, for example, by Netzer et al. (2003). The galactic absorption, empirical emission lines, and all `warmabs` parameters are kept the same in all observations.

As expected, our bare continuum model produces only a poor description of the data. We subsequently increase the number of absorption components and refit continuum as well as absorption parameters. The fit parameters for each `warmabs` component are $\log \xi$, N_H, and velocity shift. We fit for the abundances of C, N, O, Ne, Mg, Si, S, Ar, Ca, Fe, and Ni, but they are kept the same across individual absorption components. The resulting C-statistics for different numbers of `warmabs` components are given in Table 2. The best-fit parameters for the corresponding models are listed in Table 3.

We experimented with adding all individual HEG and MEG data to increase the signal-to-noise, but we failed to obtain a

---

[8] See https://cxc.cfa.harvard.edu/ciao/threads/add_grating_orders/ for details.

[9] The `xstar` database contains transitions that are flagged internally as being less robust in terms of wavelength accuracy, similar to the Chianti database. The default setup is conservative and does not include these transitions for calculating the final spectrum. We find, however, that some spectral features that appear to be missing are consistent with being due to these transitions, so we choose to include them in our fit.

[10] Note that `xstar` defines the turbulent velocity in thermal units, i.e., the $v_{\mathrm{turb}} = \sqrt{2} \, v_{\mathrm{rms}}$.

Table 2
C-statistic for Different Numbers of warmabs Absorption Components

#warmabs	C-stat/dof
0	$67967.5/41721 = 1.63$
1	$51429.1/41709 = 1.23$
2	$49590.9/41706 = 1.19$
3	$48021.8/41703 = 1.15$
4	$47500.9/41700 = 1.14$
5	$47241.3/41697 = 1.13$
combined spectra	
5	$11126.9/5636 = 1.97$

statistically acceptable fit even with five warmabs components, likely due to reported variability across individual observations. Our best C-stat/degrees of freedom (dof) for the combined spectra is ∼2, which is similar to the best fit by Mao et al. (2019) for the averaged 2000–2013 data with nine warm absorber components using the PION model in SPEX (Kaastra et al. 1996).

4. Validity Checks of the Best-fit Model

4.1. Charge State Distributions

We explore the hypothesis that a major contribution to the non-ideal fit statistics is a mismodeling of the charge state distribution, i.e., that the CSD predicted xstar/warmabs does not reproduce the real CSD accurately enough, and individual fractional ion populations are over- or underestimated.

In order to fit individual ion columns directly, we tabulated the optical depth from each ionization state of C, N, O, Ne, Mg, Si, S, Ar, Fe, and Ni as a function of energy and construct an absorption model with only these elements that allow us to fit for the column density of each ion (i.e., the total charge state distribution) directly. The best fit obtained with this procedure is C-stat/dof of $47542.34/41555 = 1.14$.

Figure 1 shows a scatter plot comparing the ion columns derived from the direct fit of the CSD (ion-by-ion) to the ion column density predicted by xstar/warmabs for Si and Fe (other elements are shown in Appendix A). This figure shows that the best-fit CSD and the equilibrium CSD agree for the more abundant ions of each element. The ion-by-ion fitted CSD generally requires greater fractional abundance for the low abundance ions than is produced by the equilibrium model. This is not surprising since equilibrium models generally produce a very steep decrease in ion fraction as a function of the ion stage for ion stages significantly above or below the ion stage with the maximum fractional abundance.

We find the largest deviations between the ion-by-ion fit and the equilibrium solution in some low-charge ions (e.g., Fe IV or Si VI which are not well constrained by absorption lines but mostly contributes to continuum absorption. Due to the large number of free parameters those ion columns rather reflect imperfections and degeneracies in the continuum modeling than robust constraints on the ionization structure.

The ion-by-ion fitted CSD model includes only a single velocity shift which makes the final fit statistics not directly comparable to those in Table 2. If we simplify our multi-component warmabs model to a single velocity shift and only include those elements of the direct CSD fit for comparison, our best fit is C-stat/dof of $47542.34/41702 = 1.16$.

We determined uncertainties from Markov Chain Monte Carlo with affine-invariant ensemble sampling (Goodman & Weare 2010; Foreman-Mackey et al. 2013) with Gaussian priors for 10 walkers per free parameter (total of 1970) and 6000 interactions (see Figure 1). The CSD that we find from ion-by-ion fits differs from the equilibrium CSD for ions that have low abundance. The ion-by-ion fit does produce a better fit than a multicomponent warmabs model to a single velocity shift and only includes those elements of the direct CSD fit, i.e., C-stat/dof = 1.14 versus 1.16, but this improvement is small compared with the difference in C-stat/dof between our best-fit model and the PKS 2155−304 calibration observation, or the simulated data. For this reason, we are confident that the direct fitting of the charge state distribution also validates our selection of the precalculated ion population files that are used by warmabs.

4.2. Acceptability of the Multicomponent warmabs Model and Final Fit Quality

With an increasing number of absorption components, the fit quality improves. Including the fourth and fifth absorption components improves the C-stat/dof from ∼1.5 to ∼1.14, and further to ∼1.13, respectively. The distribution of C-residuals demonstrates, however, that the model fits the observed spectrum well in most bins. While the fit statistics improve slightly with the inclusion of additional warm absorber components, the increment becomes notably smaller, and the comparison of the distribution of C-residuals with both a calibration and simulated observation (Figure 2) shows a remaining excess mostly of C-residuals greater than 2.

While additional warmabs components still lead to improvements in the total fit statistic at the expense of relatively few additional free parameters, we conclude from the C-residuals distribution that there is no convincing physical motivation to construct a more complex baseline model. Adding further warmabs components would only be justified if the residual spectrum contained lines that indicated the presence of an absorbing medium with a different ionization state than already present in the model. In this case, however, the free CSD model would be expected to reflect this unaccounted ionization state which is not what we observe.

Our fits with the free CSD model did not produce better fit statistics, which argues against including more warm absorber components, as their combination reproduces a charge state distribution similar to the equilibrium assumed by warmabs, but with small enhancements for low abundance ions and which do not significantly improve the fit.

We further compare the distribution of C-residuals, i.e., the signed square root of the C-statistic per spectral bin[11] to the distribution of C-residuals of simulated spectra which have C-stat/dof of ∼1.00 (to assess statistical fluctuations) and to the fit of the calibration source PKS 2155−304 (see Appendix D for details) which has a comparable number of counts. The best fit of the calibration observations of PKS 2155−304 gives a C-statistic of $103686.0/100116 = 1.04$. The resulting distributions are shown in Figure 2.

We find excellent agreement between the observed, simulated, and calibration distribution for C-residuals smaller than ∼2, along with an excess of spectral bins contributing to

---

[11] See Equation (B.5) of the xspec manual https://heasarc.gsfc.nasa.gov/xanadu/xspec/XspecManual.pdf.
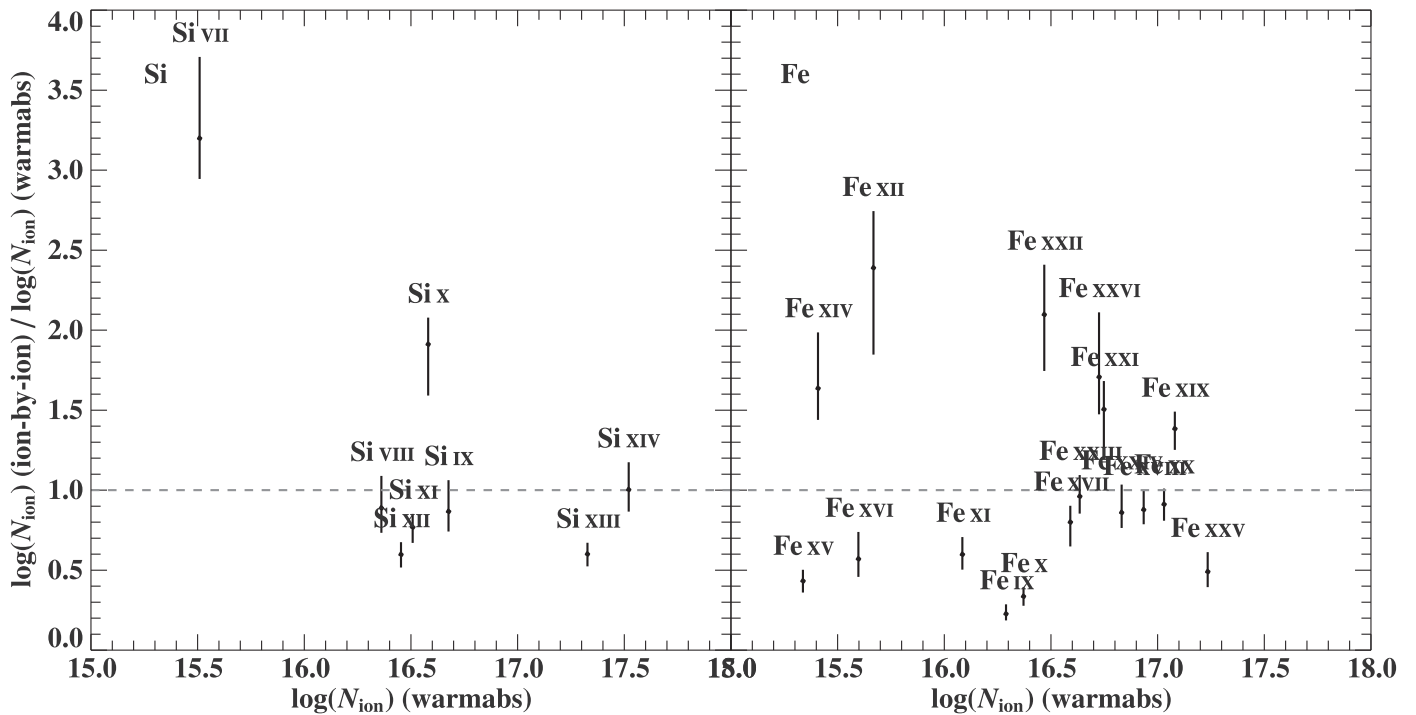
Figure 1. Scatter plot of ion column densities for Si and Fe obtained calculated by `xstar/warmabs`. Uncertainties are purely statistical and on a 90% confidence level. from direct fitting vs. the equilibrium charge state distribution.

the total C-residuals greater than ~ 2 that is basically independent of the number of absorption components for three and more absorbers. Such an excess of large C-residuals, however, would require strong, mismatching lines. We expect that a model comprising a sufficient number of absorption lines would be able to account for this by adjusting the overall charge state distribution (CSD). We note that this argument only applies to features that match a possible transition in the underlying atomic database in the first place. Since the distributions of the calibration observation and the simulated data still agree well, it is very unlikely that the discrepant bins are solely due to instrumental issues but are also an effect of the modeling.

We therefore conclude that the addition of further `warmabs` components is not justified, especially since it is not clear whether the remaining deviation of C-stat/dof from unity is only due to a mismodeling of the absorption lines or a result of other effects.

We use the five-component `warmabs` as a baseline model for our following analysis, as we do not detect any specific residual features that would indicate the presence of additional warm absorber components. To our knowledge, this is also among the best published fits for the comprehensive 2001 Chandra/HETG data of NGC 3783. However, our best C-statistic is still $\sim 13\%$, larger than expected for an ideal fit, and larger than found for PKS 2155−304, which has a comparable number of counts.

4.3. Individual Line Discrepancies

We now estimate how well individual absorption lines are reproduced by our best-fit model. To do so, we add additional absorption components with Gaussian optical depth and fixed widths (again for a v_{turb} of $150\,\mathrm{km\,s^{-1}}$) and wavelengths on top of the 500 strongest lines in our combined `warmabs` model

while we keep all continuum and `warmabs` parameters fixed. All Gaussian line centroids are fixed to the respective `xstar` database rest line wavelength value modified by a single velocity shift for all lines. We fit the optical depth of each of these additional components, which can be interpreted as a modification of the optical depth of the respective `warmabs` model line, following a similar approach presented by Gu et al. (2022) for emission lines of coronal plasmas. We note that since the additional Gaussian lines are tied to the database wavelengths, they cannot account for features that are missing in the database or have inaccurate reference wavelengths. We allow the Gaussian normalization to be either negative or positive, which reflects a decrease or increase in the optical depth of the model line, respectively. Allowing for the modification of these lines improves the C-statistic of our fit to $45130.1/41251 = 1.09$. Figure 3 shows the $10.5\,\text{Å}–11.0\,\text{Å}$ of observation 2090 to illustrate this approach.

Uncertainties on the additional optical depths are obtained with standard C-statistic minimization techniques. This is technically feasible because, unlike the measurement of the CSD, this is a local problem to the respective line. It is therefore sufficient to consider only a narrow wavelength range. Due to the known continuum variability of NGC 3783 (e.g., Netzer et al. 2003), we refrain from combining individual spectra for our fit.

We now compare the additional optical depth added to each line with the optical depth that the `warmabs` model predicts. Figures 4, 5, and 6 show the additional optical depth fitted for each of the 500 strongest model lines and the distribution of optical depth modifications. We find that most lines require rather small modifications and do not observe a strong correlation between τ and $\Delta\tau$. This is in line with our expectation that for weak lines, the total uncertainty of the line's optical depth is rather dominated by statistical rather than systematic uncertainties. We further find that the additional
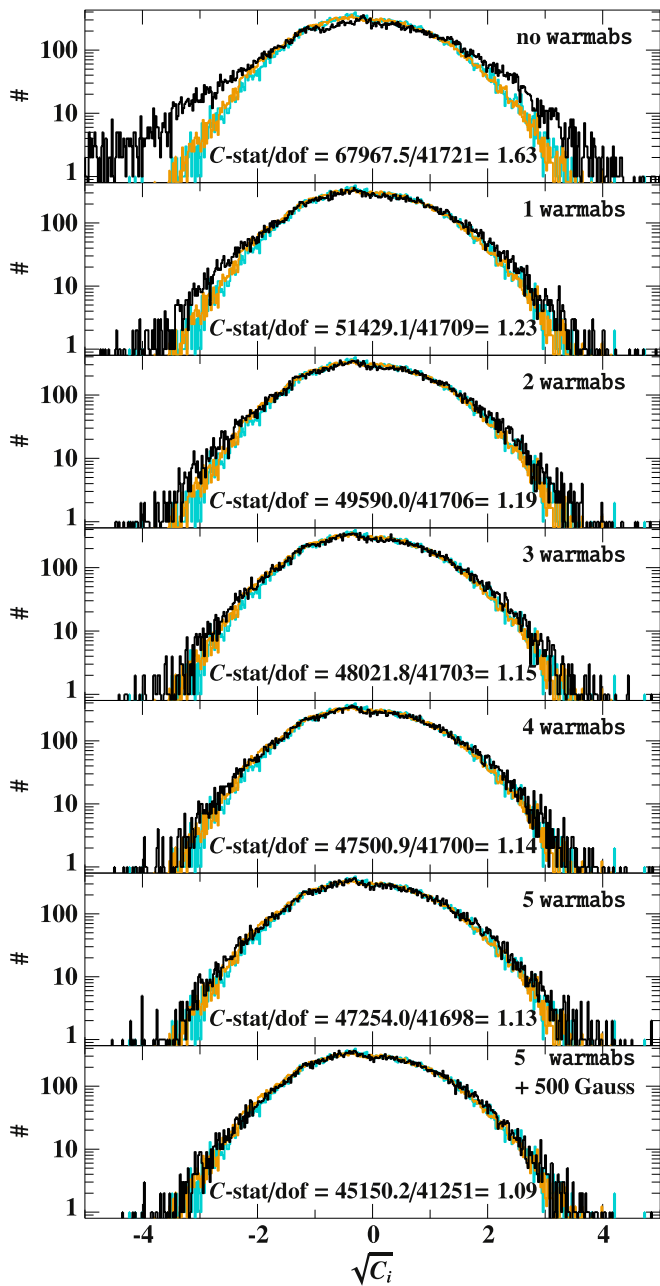
Figure 2. Distribution of C-residuals (square root of C-statistic per bin, signed according to data model) for our different trial models (black), a simulated spectrum based on our best-fit model (cyan), and a set of calibration observations of PKS 2155−304 (orange).

optical depth is sharply peaked around $\Delta\tau \simeq 0$. Figure 5 and 6 also shows that there appears to be a slight excess of lines with $\Delta\tau < 0$ compared with $\Delta\tau > 0$. This makes sense for absorption lines, since saturation effects would tend to make the line equivalent width less sensitive to increases in the line optical depth and more sensitive to decreases. The importance of this effect will increase for more optically thick lines. Results shown here suggest that it is still important for lines with small or moderate optical depth.

4.4. Model Uncertainties

We compare our results with an experimental version of warmabs that takes into account uncertainties on the radiative

transition rates. That is, we take the values of $\Delta\tau/\tau$, as shown in Figure 4, and use them to derive fractional uncertainties in the Einstein A-values for those lines. These A-value uncertainties are included in the xstar atomic database. In doing so, we include the constraint that the A-value cannot become negative. We then incorporate the A-value uncertainties into warmabs by calculating each line spectrum three times: once for the most probable A-values, and once each for the maximum and minimum A-values implied by the uncertainties. For each wavelength bin in our model spectrum we calculate the difference between the models calculated with the most probable A-value and the maximum and minimum allowed A-values; we adopt for the model uncertainty in each wavelength bin the greater of these quantities. This array of model uncertainty versus wavelength bin is returned by warmabs to xspec.

Here and for subsequent comparisons we adopt χ^2 statistics because C-statistics inherently cannot accommodate model uncertainties as the variance is a direct consequence of the Poisson process. In xspec,[12] any additional model variance is added to the data variance so that the modified fit statistics for a multiplicative model with model variance ΔM_i for bin i is

$$\chi^2 = \sum_{i=1}^{N} \frac{(d_i - m_i)^2}{\sigma_i^2 + m_i^2 \Delta M_i} , \qquad (1)$$

where d_i and m_i are the data and model counts in bin i, respectively, and σ_i is the data uncertainty. For a Poisson-distributed process, the contribution of the model uncertainty will dominate over the Poisson uncertainty for bins with counts $m_i \gtrsim (\Delta M)^{-1}$. The effect of model uncertainty on a spectral fit will therefore depend strongly on the details of the modeled spectrum.

To illustrate how model uncertainties become relevant for statistically high-quality spectra, we simulated spectra for different exposures based on the MEG response and for our NGC 3783 continuum model. We did this as an illustrative test, using an absorber that contains only oxygen with $\log\xi = 1$ which produces O VII and O VIII lines. These lines have uncertainties associated with them from the procedure described in Section 4.3. The optical depth distribution for $\log\xi = 1$ and $N_H = 10^{21}\,\mathrm{cm}^{-2}$ is shown in Figure 7 along with the distribution of model uncertainties.

One important result is that, even for high-count spectra, model uncertainties dominate only the core of strong absorption lines. That is, the model uncertainties are small in the spectral regions away from the cores of these lines. As a consequence, the inclusion of model uncertainties may improve data model residuals for individual lines but is unlikely to change fit results substantially for spectra containing a large set of absorption lines of different elements.

To assess the effect of model uncertainties on derived plasma parameters we simulated absorption spectra for the order +1 MEG response assuming the NGC 3783 continuum model with a single oxygen absorber. We varied the simulated exposure time and determined the uncertainty of the ionization parameter using the warmabs model described above with and without model uncertainties. Figure 8 shows the fractional uncertainty of the ionization parameter obtained from these simulations as a function of exposure or number of counts in the center bin of

---

[12] See Appendix B of the xspec manual for a definition of the fit statistics (https://heasarc.gsfc.nasa.gov/xanadu/xspec/XspecManual.pdf).
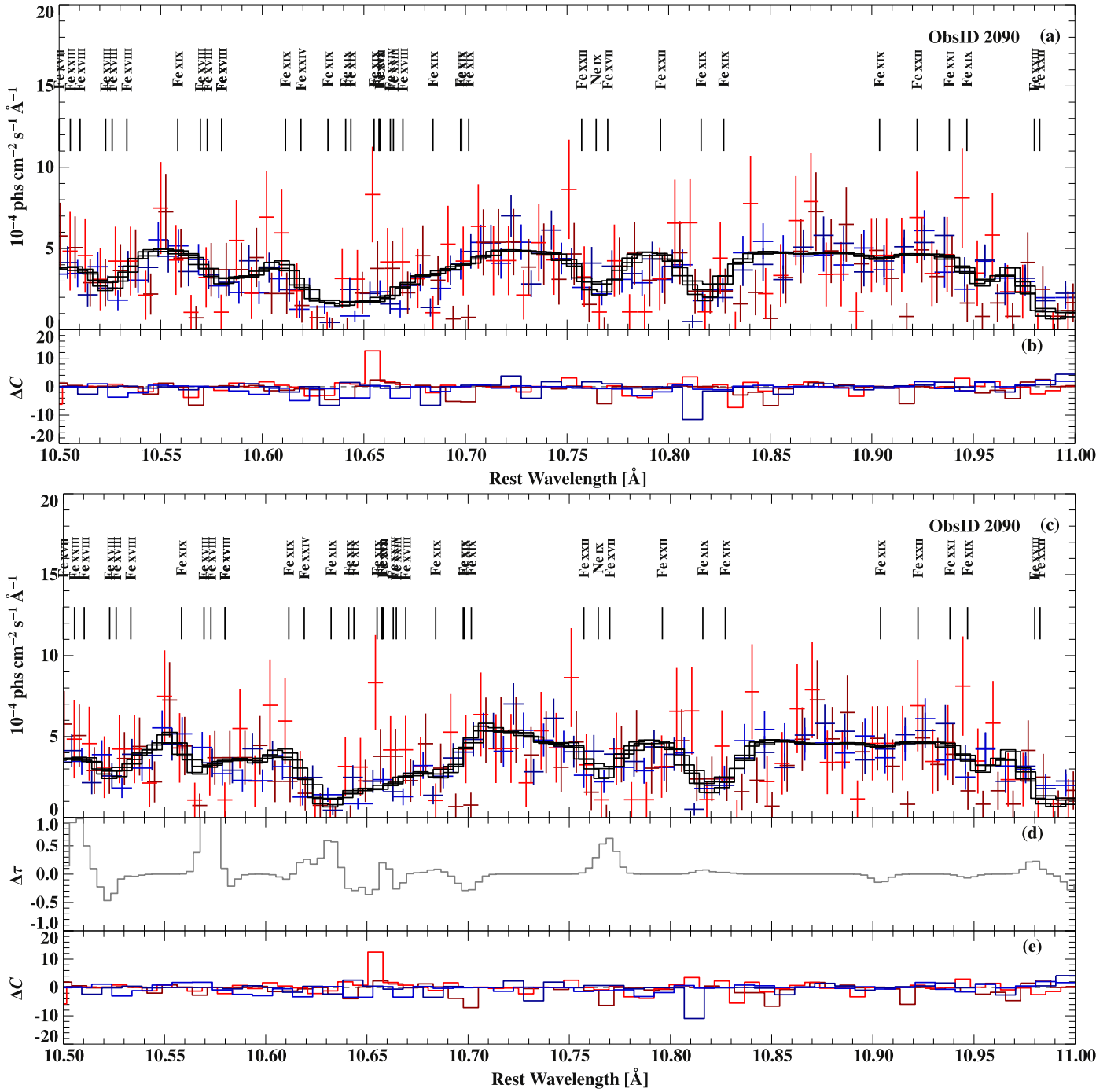
Figure 3. (a) Close-up of the HEG (red) and MEG (blue) 10.5–11.0 Å spectra of the NGC 3783 observation 2090 fitted with a five-component `warmabs` model (black). (b) C-residuals for the baseline model. (c) Same data as in (a) but with the `warmabs` model modified by the additional Gaussian lines. (d) Additional optical depth $\Delta\tau$ that is added or removed from each bin by the Gaussian components. (e) C-residuals for the modified model. As shown here and described in Section 5.1, including additional Gaussians—equivalent to modifying A-values for the strongest 500 lines—leads only to minor to moderate improvement of the fit statistics and residuals.

the O VIII Lyα line. While this simulation is a strong simplification of a real observation where generally a larger sample of elements is observed simultaneously with different instruments and grating orders, it illustrates that even for grating spectra with high statistical quality (typical observing times of a few hundred ks) we expect inclusion of model uncertainties to improve the confidence intervals on plasma parameters by only a few percent.

5. Discussion

5.1. Validation of Baseline Model and Final Fit Quality

The distribution of C-residuals demonstrates that the model fits the observed spectrum well in most bins. We obtain a final C-stat/dof of $\sim$1.13 for five warm absorber components. While the fit statistics improve slightly with the inclusion of additional warm absorber components, the increment becomes notably
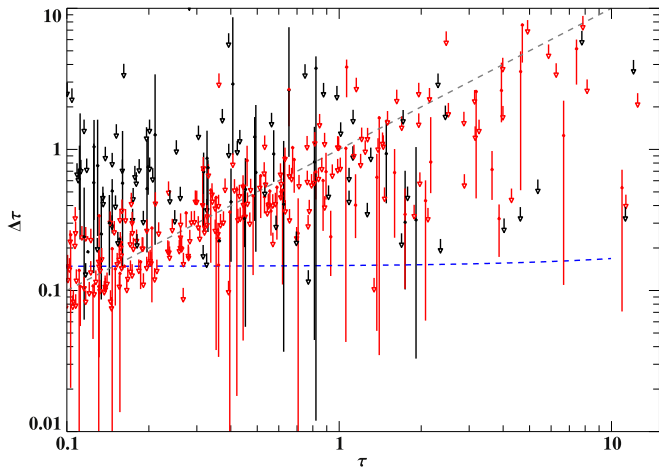
Figure 4. Additional optical depth for each of the 500 lines from the Gaussian components against the optical depth of the model line without the Gaussian component. Black data points show positive additional optical depth (i.e., the absorption line becomes stronger), and red shows negative additional optical depth (i.e., the absorption line becomes weaker). The gray dashed line marks $\Delta\tau = \tau$, and the blue dashed line is a linear regression to the τ vs. $\Delta\tau$ relation. The 90% upper limits are shown by a downward pointing error with the limit given at the base of the arrow. Of the 500 lines, 390 are upper limits, and 110 are detections.
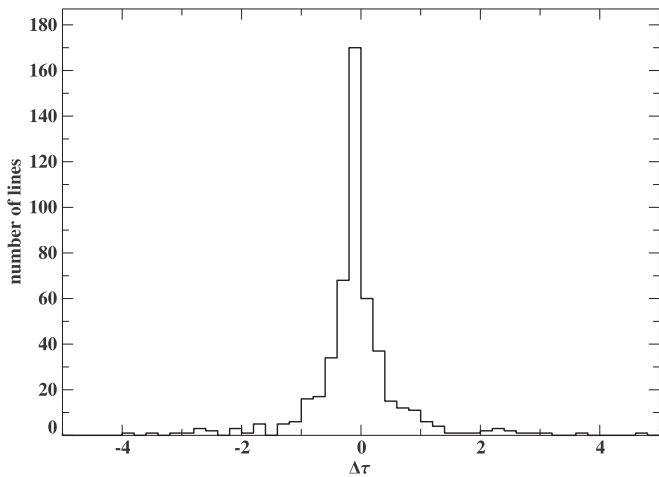

Figure 5. Normalized distribution of absolute contributions of the 500 strongest model lines.

Figure 6. Normalized cumulative histogram of the 500 line modifications. Black data points show positive additional optical depth (i.e., the absorption line becomes stronger), and red shows negative additional optical depth (i.e., the absorption line becomes weaker).

Figure 7. Top: simulated MEG +1 spectrum with 10^9 s exposure, based on our NGC 3783 continuum model with a single oxygen absorber with $\log\xi = 1$ and $N_{\rm H} = 10^{21}$ cm^{-2}. The gray shaded region shows the total uncertainty associated with each bin. Bottom: fractional uncertainty of each bin for the Poisson uncertainty (red) and the model uncertainty (blue).

smaller, and the comparison of the distribution of *C*-residuals with both a calibration and simulated observation (Figure 2) shows a remaining excess mostly of *C*-residuals greater than 2.

While additional `warmabs` components still lead to improvements in the total fit statistic at the expense of relatively few additional free parameters we conclude from the *C*-residuals distribution that there is no convincing physical motivation to construct a more complex baseline model. Adding further `warmabs` components would only be justified if the residual spectrum contained lines that indicated the presence of an absorbing medium with a different ionization state than already present in the model. In this case, however, the free CSD model would be expected to reflect this unaccounted ionization state which is not what we observe.

Our fits with the free CSD model did not produce better fit statistics, which argues against including more warm absorber components, as their combination reproduces a charge state distribution similar to the equilibrium assumed by `warmabs`,
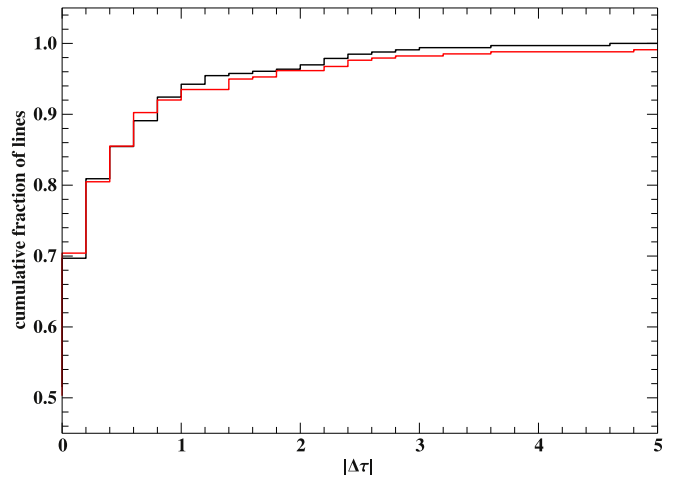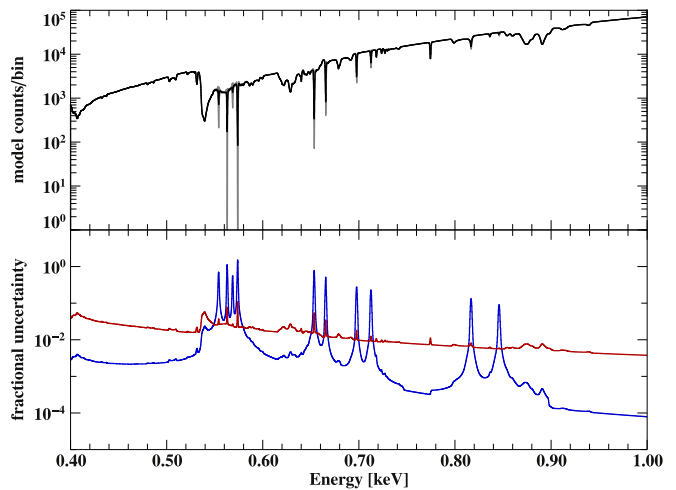
but with small enhancements for low abundance ions and which do not significantly improve the fit.

Allowing for modifications for the 500 strongest lines does improve *C*-residuals distribution, as expected, since mismatches in individual, strong lines can be accounted for. However, a significant excess of large *C*-residuals remains that appear to be stochastically distributed and not associated with missing edges or lines. If these were due to absorption features that are missing in the `xstar` database, we would expect them to show up clearly in the spectra. On the other hand, lines so weak that do not have a corrective Gaussians assigned to them are unlikely to produce such large residuals though this remains a possibility that cannot fully rule out. Also, lines that are not in the xstar database or which have inaccurate wavelengths could provide some of the *C*-stat/dof.

The remaining sources for data model discrepancies are systematics in our model that cannot be accounted for by a modification of the optical depth of strong absorption lines. Such systematics could be in the reference wavelengths in the
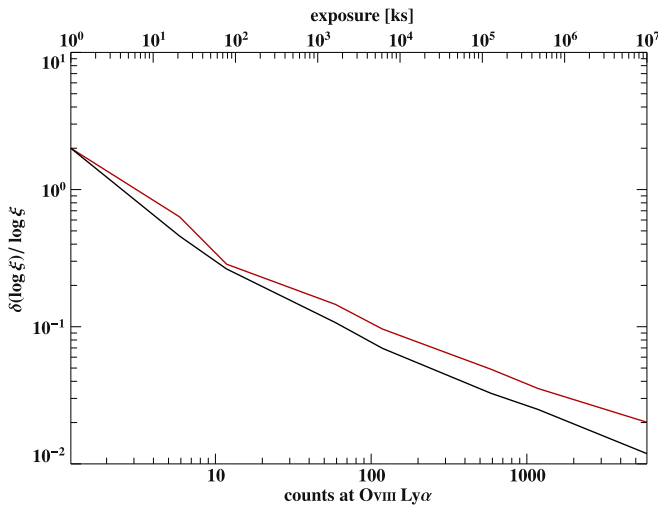
Figure 8. Fractional uncertainty on the ionization parameter in simulated spectra as a function of signal-to-noise ratio per resolution element at the center of the O VIII Lyα line (for $R = 1000$) for the standard `warmabs` model (black) and the version including model uncertainties (red).

database, detector calibration uncertainties, e.g., in the line response function, emission features not included in the model, mismodeling of the background, or short-term variability of the source.

Of these, inaccuracies in the reference wavelengths are not expected for the very strongest lines, since most of these utilize wavelengths that have been measured in the laboratory (Brown et al. 2002; Deslattes et al. 2003). On the other hand, it is possible that the cumulative effect of wavelength inaccuracies in many weak lines could make a significant contribution to the C-stat/dof that we find. If so, significant effort would be required in order to remedy this for many weak lines.

Detector calibration uncertainties appear to be an unlikely explanation for the fit statistic that we find, since we obtain nearly perfect C-stat/dof for simulated data and for the PKS 2155−304 observation. It is possible that the presence of many absorption lines in the NGC 3783 spectrum causes the C-stat/dof to depend on the detector calibration in a different way than for PKS 2155−304. Inaccuracies in the line spread function, or the effects of scattered light in the cores of absorption lines, could affect the NGC 3783 fits more than the PKS 2155−304 fits.

5.2. Distribution of Corrective Optical Depth $\Delta\tau$

Figure 4 shows that the distribution of line uncertainties is more independent from τ than found by Gu et al. (2022) for emission lines in coronal models. We note that for only 110 out of 500 absorption line uncertainties on the additional optical depth, $\Delta\tau$ could be constrained, whereas for the remaining lines only upper limits could be obtained. A linear regression of the magnitude of $\Delta\tau$ versus τ (blue curve in Figure 4 results in only a very small positive correlation with a slope that is consistent with zero within its uncertainty. This dependence appears to be consistent with the effects of measurement errors of the optical depths of the absorption lines, which would predict that the uncertainties become harder to measure for weaker lines and so that $\Delta\tau$ versus τ would be flat or increasing at small τ. Similarly, the atomic data (A-values) for weaker lines might be expected to be more difficult to calculate, which would also be expected to produce greater

$\Delta\tau$ for smaller τ. For most of the absorption lines, a modification of the optical depth does not lead to a significant improvement in the fit.

5.3. Implementation into X-Ray Spectral Analysis Packages

Distribution of the complete estimated uncertainties of the radiative rates used in this work will happen through regular updates of the `xstar`/`warmabs` database.[13] Table 4 lists derived relative uncertainies on a few selected lines for illustration. Propagated model uncertainties can be used directly in all X-ray spectral analysis packages that provide an interface for compiled `xspec` third-party models.

We consider this a complementary approach to `AtomDB`/ `APEC` and `SPEX`/CIE. `AtomDB`/`APEC` released routines in their Python package `PyAtomDB`[14] (Foster & Heuer 2020; Foster 2020; Heuer et al. 2021) that employ a Monte Carlo approach to calculate uncertainties of the CSD by repeated stochastic perturbations of collisional rates.

Gu et al. (2022) also use high-quality observational data to quantify necessary corrections to individual lines, but instead of including those in the atomic database, they derive an empirical uncertainty relation for line emissivities. Systematic uncertainties of fit parameters of `SPEX`/CIE for a given observation are then obtained from large-scale simulations. Those simulated spectra are precalculated for performance increase but limit the number of accessible parameters. This approach specifically focuses on key parameters such as kT, norm, and abundances, enabling computing the error swiftly and with minimal computational overhead.

6. Conclusions and Outlook

We reanalyzed a set of archival Chandra/HETG observations of NGC 3783 and modeled the warm absorber in this source with the `xstar`-derived absorption model `warmabs` in order to characterize the quality of the photoionization model and the underlying atomic data, and to understand the remaining data model residuals that often lead to statistically poor fits. In particular, we start from a baseline model that includes five `warmabs` components that we expect to account for all major photoionized absorbing components in NGC 3783. We compared this fit of a self-consistent photo-ionization model to a manually constructed absorption model where the charge state distribution is fitted directly without any equilibrium constraints. We compared the charge state distribution obtained with both models and the final fit statistics. The free charge state model produces in fact slightly worse fit statistics than our baseline model, mostly because of a more simplistic treatment of the velocity shifts. We therefore conclude that the final quality of fit in this stage is rather affected by inaccuracies of the line profile modeling and that the overall charge state distribution is well constrained by the comprehensive set of absorption lines. In a second step, we allowed individual lines of our best-fit model to vary in optical depth to account for the plausible possibility of inaccurate radiative transition rates for some of the model lines. This approach leads to a modest improvement of the fit statistic of the order of about 5% and the distribution of C-residuals larger than 2 is still not ideal.

---

[13] https://heasarc.gsfc.nasa.gov/xstar/xstar.html
[14] https://github.com/AtomDB/pyatomdb

We conclude that inaccuracies of radiative transition rates are not a major source of data model discrepancies. Our fits to simulated spectra further show that in the majority of practical cases of currently available observational data, statistical uncertainties dominate the accuracy to which plasma parameters can be constrained. Including model uncertainties in `warmabs` leaves us with the conclusion that unsatisfactory spectral fits cannot be attributed solely to uncertainties in radiative transition rates in the atomic databases. Our comparison with the free CSD model further confirms that the approach of `warmabs` to employ precalculated ion population files is sufficient for the available data quality.

This result raises the question of other sources of data model discrepancies that are likely to be common in modeling photoionized material. Regarding the quality of the atomic databases, we emphasize that our approach can only account for mismatches associated with bound–bound radiative transitions that are listed in the `xstar` database. Radiative bound–bound transitions that are missing completely from the database would not have been captured by our approach since there is no reference line to adjust, nor uncertainties of the transition wavelength. Determining and accounting for wavelength mismatches is mostly limited by line blends and detector resolution, and we expect major improvements in wavelength benchmarking by microcalorimeter missions like XRISM and Athena. At the current resolution, we would expect wavelength inaccuracies to result in a deformation of the line profile, which cannot be disentangled easily from detector calibration issues or complex outflow velocity profiles.

Beyond the quality of the atomic database, we expect the major origin of data model discrepancies to be the applicability of the model itself, i.e., whether the degree of simplification inherent to any model is appropriate for the present source. In this case, the pure absorption model `warmabs` cannot account for any of the observed emission lines. While we can easily describe these lines empirically, this clearly points toward a limited understanding of the true conditions of the reprocessing material, which might introduce other unknown systematic effects. This is really the true goal of observational science anyway: the testing and falsification of models, and so it should provide important clues about the true conditions in cosmic sources.

While our work validates results obtained with previous versions of `warmabs`, we expect future microcalorimeter missions like XRISM and Athena to reveal further inaccuracies of atomic data products that will have to be accounted for in the process of analyzing their spectral data. Ongoing efforts in improving both atomic structure calculations and experimental benchmarking are unlikely to resolve all remaining uncertainties for the majority of atomic data products in the next several years.

The way model uncertainties can be estimated quantitatively is not unique, and we consider our approach based on observational line opacities just one of several possibilities, e.g., a comparison between different atomic codes or experimental measurement uncertainties. We therefore expect a further refinement of the transition rate uncertainties in future releases of the database. With the continuous improvement of observational data quality, we expect model uncertainties to become more and more relevant for any sophisticated, physically motivated spectral model, not limited to photoionized plasmas. As we have demonstrated, the statistical treatment and the implications of model uncertainties are by no means trivial, and a major investment will be necessary to improve our understanding of their application. The X-ray data analysis package `SPEX` has implemented atomic data uncertainties and estimates on their contribution to the derived plasma parameters of their CIE model based on precalculated uncertainties (see Gu et al. 2022). To our knowledge, `xspec` is currently the only X-ray data analysis package that has an interface to process model uncertainties directly and propagate them through the calculation of the fit statistics.

Appendix A
CSD for Individual Elements

A major assumption of our modeling approach is that the total optical depth of the absorbing medium is only moderate at most, and therefore ionization gradients are negligible, as these would also affect observed line depths. In order to verify this assumption, we compare our equilibrium CSD with a direct fit of CSD where all ion populations are allowed to vary freely. Figure 9 shows the comparison of the ion column densities for various elements.
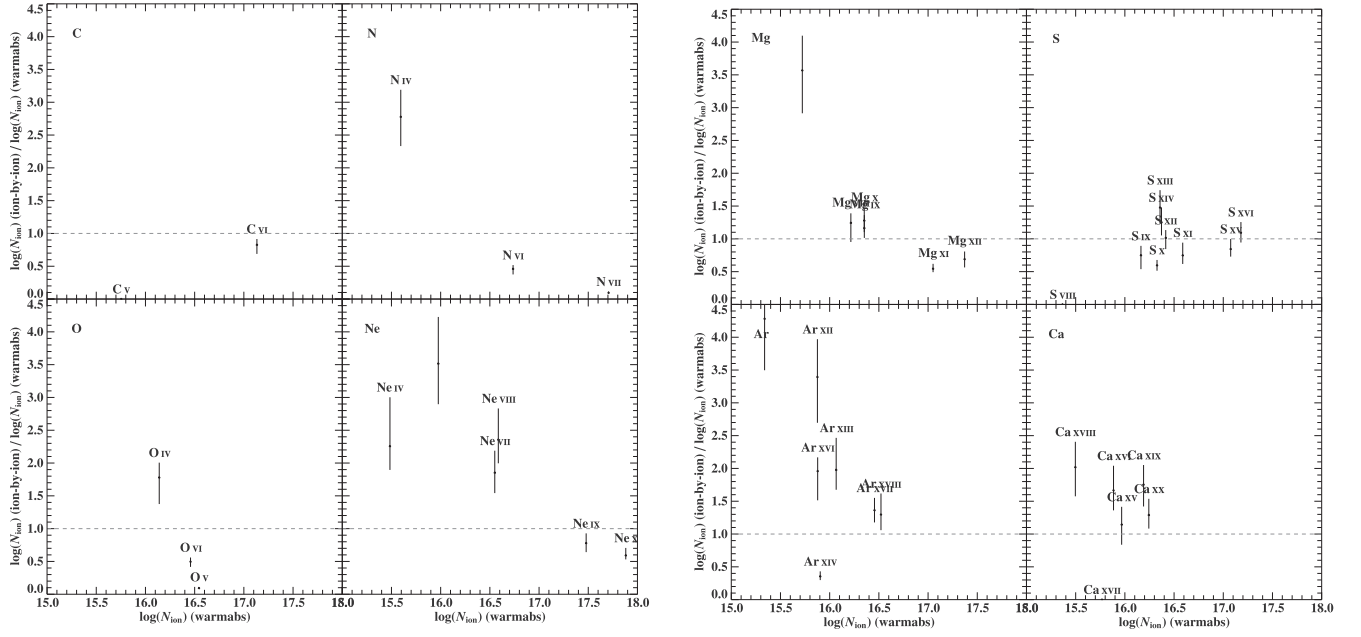
Figure 9. Scatter plot of ion column densities for C, N, O, Ne, Mg, S, Ar, and Ca obtained from direct fitting vs. xstar/warmabs. Uncertainties are purely statistical and on a 90% confidence level.

Appendix B
Table of Best-fit Parameters

Table 3 provides the comprehensive set of fit parameters for the different multicomponent models.

Table 3
Best-fit Parameters for the Baseline Models with One to Five `warmabs` Components

Parameter	1 warmabs	2 warmabs	3 warmabs	4 warmabs	5 warmabs
N_H [a]	$0.195^{+0.007}_{-0.006}$	0.181 ± 0.005	$0.134^{+0.025}_{-0.014}$	0.131 ± 0.001	0.092 ± 0.002
$\log(N_H)_1$ [b]	$0.46^{+0.05}_{-0.07}$	0.375 ± 0.018	0.26 ± 0.15	$-0.219^{+0.005}_{-0.006}$	$-0.362^{+0.012}_{-0.013}$
$\log \xi_1$	2.24 ± 0.01	2.19 ± 0.02	$2.23^{+0.26}_{-0.32}$	1.53 ± 0.01	$1.50^{+0.04}_{-0.08}$
v_1 [c]	-680 ± 8	-702^{+14}_{-13}	-700^{+60}_{-120}	-729^{+5}_{-6}	-727^{+39}_{-16}
$\log(N_H)_2$ [b]	⋯	$0.483^{+0.023}_{-0.022}$	$-0.27^{+0.09}_{-0.20}$	0.244 ± 0.010	$0.116^{+0.012}_{-0.013}$
$\log \xi_2$	⋯	2.94 ± 0.01	$1.5^{+0.5}_{-0.4}$	2.24 ± 0.02	2.23 ± 0.01
v_2 [c]	⋯	-597^{+7}_{-8}	-750^{+60}_{-130}	-676 ± 5	-676^{+12}_{-9}
$\log(N_H)_3$ [b]	⋯	⋯	$0.34^{+0.07}_{-0.12}$	0.279 ± 0.004	$0.149^{+0.016}_{-0.012}$
$\log \xi_3$	⋯	⋯	$2.96^{+0.23}_{-0.27}$	2.96 ± 0.01	$2.97^{+0.01}_{-0.02}$
v_3 [c]	⋯	⋯	-580^{+230}_{-650}	-566 ± 6	-544^{+9}_{-23}
$\log(N_H)_4$ [b]	⋯	⋯	⋯	-0.062 ± 0.004	$-0.210^{+0.008}_{-0.010}$
$\log \xi_4$	⋯	⋯	⋯	3.05 ± 0.01	3.04 ± 0.03
v_4 [c]	⋯	⋯	⋯	-1359 ± 4	-1335 ± 8
$\log(N_H)_5$ [b]	⋯	⋯	⋯	⋯	$-1.167^{+0.008}_{-0.010}$
$\log \xi_5$	⋯	⋯	⋯	⋯	-0.20 ± 0.04
v_5 [c]	⋯	⋯	⋯	⋯	-1452^{+8}_{-7}
a_C	$1.3^{+1.0}_{-1.2}$	1.14 ± 0.04	$0.5^{+0.9}_{-0.5}$	0.44 ± 0.02	$0.27^{+0.04}_{-0.03}$
a_N	$5.00^{+0.05}_{-0.12}$	$5.00^{+0.09}_{-0.11}$	$2.5^{+2.0}_{-1.0}$	4.47 ± 0.01	1.43 ± 0.03
a_O	$4.2^{+0.6}_{-0.5}$	3.0 ± 0.03	$1.9^{+1.7}_{-1.2}$	1.83 ± 0.01	$2.24^{+0.02}_{-0.03}$
a_{Ne}	$1.39^{+0.18}_{-0.14}$	1.05 ± 0.06	0.9 ± 0.4	0.99 ± 0.02	$1.48^{+0.01}_{-0.02}$
a_{Mg}	$0.79^{+0.11}_{-0.10}$	0.63 ± 0.06	0.8 ± 0.6	0.78 ± 0.01	$1.05^{+0.02}_{-0.03}$
a_{Si}	$1.39^{+0.20}_{-0.15}$	$0.98^{+0.04}_{-0.07}$	$1.4^{+1.2}_{-0.9}$	1.26 ± 0.02	$1.71^{+0.03}_{-0.4}$
a_S	$1.06^{+0.16}_{-0.14}$	0.77 ± 0.04	$1.0^{+1.3}_{-1.4}$	0.95 ± 0.01	$1.27^{+0.02}_{-0.03}$
a_{Ar}	$0.79^{+0.22}_{-0.12}$	1.10 ± 0.04	$1.1^{+0.8}_{-0.7}$	1.14 ± 0.02	$1.45^{+0.01}_{-0.02}$
a_{Ca}	$0.4^{+0.8}_{-0.7}$	0.79 ± 0.04	$1.3^{+2.1}_{-0.6}$	1.23 ± 0.01	$1.90^{+0.05}_{-0.03}$
a_{Fe}	$0.51^{+0.08}_{-0.06}$	0.47 ± 0.05	$0.7^{+0.5}_{-0.4}$	0.67 ± 0.01	$0.93^{+0.03}_{-0.02}$
a_{Ni}	0.61 ± 0.12	$0.70^{+0.04}_{-0.02}$	$1.0^{+1.1}_{-1.3}$	1.02 ± 0.02	$1.43^{+0.06}_{-0.05}$
z [d]	9.48 ± 0.11	$9.44^{+0.09}_{-0.10}$	$9.4^{+0.8}_{-1.3}$	9.34 ± 0.02	$9.32^{+0.04}_{-0.03}$
$E_{Fe\ K\alpha}$ [e]	6.40 ± 0.01	6.40 ± 0.01	6.40 ± 0.01	6.40 ± 0.01	6.40 ± 0.01

Table 3
(Continued)

Parameter	1 warmabs	2 warmabs	3 warmabs	4 warmabs	5 warmabs
$A_{Fe\ K\alpha}$ [f]	6.0 ± 0.6	5.4 ± 0.6	5.0 ± 1.2	5.0 ± 0.6	5.4 ± 0.6
A_{G2} [f]	3.4 ± 0.6	$3.4^{+0.8}_{-0.7}$	$3.2^{+3.8}_{-2.4}$	$3.3^{+2.4}_{-2.2}$	3.3 ± 1.0
A_{G3} [f]	$4.3^{+1.0}_{-0.9}$	4.1 ± 1.1	$4.1^{+4.8}_{-2.9}$	$4.0^{+0.9}_{-0.8}$	$3.7^{+2.2}_{-1.8}$
A_{G4} [f]	1.46 ± 0.23	$1.35^{+0.28}_{-0.26}$	1.2 ± 0.7	1.2 ± 0.6	$1.11^{+0.25}_{-0.24}$
A_{G5} [f]	0.60 ± 0.11	$0.60^{+0.13}_{-0.12}$	0.5 ± 0.4	$0.55^{+0.20}_{-0.19}$	$0.57^{+0.17}_{-0.15}$
A_I^{BB} [f]	...	$1.31^{+0.07}_{-0.06}$	...	1.53 ± 0.02	$4.60^{+0.04}_{-0.05}$
kT_I [e]	...	0.051 ± 0.005	...	0.044 ± 0.002	0.039 ± 0.001
A_I^{PL} [h]	1.04 ± 0.02	1.02 ± 0.02	$1.05^{+0.15}_{-0.08}$	1.07 ± 0.01	1.09 ± 0.01
Γ_I	1.44 ± 0.02	1.43 ± 0.01	$1.45^{+0.09}_{-0.04}$	1.46 ± 0.01	1.47 ± 0.01
A_{II}^{BB} [f]	...	...	...	...	...
kT_{II} [e]	...	...	...	...	...
A_{II}^{PL} [h]	0.97 ± 0.02	0.95 ± 0.02	$0.98^{+0.41}_{-0.23}$	1.00 ± 0.08	1.03 ± 0.03
Γ_{II}	1.51 ± 0.02	1.49 ± 0.02	$1.48^{+0.63}_{-0.27}$	1.48 ± 0.02	$1.50^{+0.03}_{-0.02}$
A_{III}^{BB} [f]	...	$0.57^{+0.25}_{-016}$	...	...	...
kT_{III} [e]	...	$0.1^{+1.2}_{-0.4}$	...	...	...
A_{III}^{PL} [h]	1.22 ± 0.03	$1.20^{+0.04}_{-0.03}$	$1.24^{+0.28}_{-0.22}$	1.27 ± 0.07	1.28 ± 0.03
Γ_{III}	1.54 ± 0.02	$1.53^{+0.11}_{-0.05}$	$1.56^{+0.30}_{-0.19}$	1.57 ± 0.02	1.57 ± 0.02
A_{IV}^{BB} [f]	...	...	$4.5^{+4.1}_{-1.2}$	...	...
kT_{IV} [e]	...	...	$0.1^{+6.7}_{-2.8}$	...	...
A_{IV}^{PL} [h]	2.20 ± 0.05	2.17 ± 0.05	$2.20^{+0.38}_{-0.27}$	$2.23^{+0.11}_{-0.12}$	2.24 ± 0.05
Γ_{IV}	1.73 ± 0.03	1.72 ± 0.02	$1.73^{+0.10}_{-0.14}$	1.73 ± 0.02	1.74 ± 0.02
A_V^{BB} [f]	...	...	...	$0.51^{+1.02}_{-0.23}$	...
kT_V [e]	...	...	...	$0.07^{+0.25}_{-0.28}$	...
A_V^{PL} [h]	1.39 ± 0.03	$1.38 \pm +0.03$	$1.42^{+0.20}_{-0.17}$	1.45 ± 0.05	$1.46^{+0.05}_{-0.04}$
Γ_V	1.50 ± 0.02	1.49 ± 0.02	1.52 ± 0.10	1.53 ± 0.01	$1.53^{+0.04}_{-0.03}$

Notes.
[a] `tbabs` absorption column density in units of $10^{22}\ cm^{-2}$.
[b] Log of the `warmabs` column density in units of $10^{22}\ cm^{-2}$.
[c] In units of $km\ s^{-1}$.
[d] Redshift in units of 10^{-3}.
[e] Energy in units of keV.
[f] In units of $10^{-5}\ phs\ cm^{-2}\ s$.
[g] Blackbody luminosity in units of $10^{36}\ erg\ s^{-1}$ at a distance of 10 kpc.
[h] In units of $10^{-2}\ phs\ keV^{-1}\ cm^{-2}\ s^{-1}$ at 1 keV.

Table 4
Example of Some of the Model Lines with Associated Uncertainties

Ion	Transition	Wavelength [Å]	τ	$\Delta\tau/\tau$
O VII	$1s1.2p1.1P_1 - 1s2.1S_0$	21.602	59.98	−0.01
Ne IX	$1s1.2p1.1P_1 - 1s2.1S_0$	13.447	17.07	−0.11
Ne X	$1s0.2p1.2P_1/2 - 1s1.2S_1/2$	12.137	8.13	−0.27
Ne X	$1s0.2p1.2P_3/2 - 1s1.2S_1/2$	12.132	15.73	−0.02
Ne X	$1s0.3p1.2P_1/2 - 1s1.2S_1/2$	10.240	1.27	−0.12
Ne X	$1s0.3p1.2P_3/2 - 1s1.2S_1/2$	10.239	2.52	−0.47
Ne X	$1s0.4p1.2P_1/2 - 1s1.2S_1/2$	9.709	0.44	−0.12
Ne X	$1s0.6p1.2P - 1s1.2S_1/2$	9.378	0.34	−0.83
Ne X	$1s0.5p1.2P_1/2 - 1s1.2S_1/2$	9.481	0.21	0.84
Mg XI	$1s1.2p1.1P_1 - 1s2.1S_0$	9.169	5.36	0.06
Mg XI	$1s1.3p1.1P_1 - 1s2.1S_0$	7.851	0.93	−0.26
Mg XI	$1s1.4p1.1P_1 - 1s2.1S_0$	7.474	0.33	0.21
Mg XI	$1s1.5p1.1P_1 - 1s2.1S_0$	7.310	0.15	−0.44
Mg XII	$1s0.2p1.2P_1/2 - 1s1.2S_1/2$	8.425	2.07	−0.21
Mg XII	$1s0.2p1.2P_3/2 - 1s1.2S_1/2$	8.419	4.03	0.01
Si XIII	$1s1.2p1.1P_1 - 1s2.1S_0$	6.648	3.86	−0.08
Si XIII	$1s1.4p1.1P_1 - 1s2.1S_0$	5.405	0.25	0.36
Si XIII	$1s1.3p1.1P_1 - 1s2.1S_0$	5.681	0.70	0.04
Si XIV	$1s0.2p1.2P_1/2 - 1s1.2S_1/2$	6.186	1.09	0.26
Si XIV	$1s0.2p1.2P_3/2 - 1s1.2S_1/2$	6.180	2.12	−0.00

Appendix C
Derived Line Uncertainties

Table 4 provides an excerpt of model lines with associated relative uncertainties. The comprehensive list is distributed within the xstar database.

Appendix D
Calibration Observations of PKS 2155−304

We extract all available Chandra/HETG data of the blazar PKS 2155−304 (Observation IDs 337, 3706, 6926, 5173, 8380, 7291, 3167, 1014, 8436, 9705, 9712, 1705, 3708), with a total exposure of ∼289.5 ks and a total of ∼5.74×10^5 counts in the MEG and ∼2.01×10^5 counts in the HEG which is comparable to total number of counts in the NGC 3783 spectra. We apply the same data extraction procedures and rebinning criteria as described in Section 2. We further exclude a small wavelength region around known O VII and O VIII absorption lines (e.g., Hagihara et al. 2010). Our fit model is an absorbed power law where photon index and normalization are independent across individual observations.

ORCID iDs

R. Ballhausen https://orcid.org/0000-0002-1118-8470
T. R. Kallman https://orcid.org/0000-0002-5779-6906

L. Gu ⬡ https://orcid.org/0000-0001-9911-7038
F. Paerels ⬡ https://orcid.org/0000-0001-9225-6481

References

Arnaud, K. A. 1996, in ASP Conf. Ser. 101, Astronomical Data Analysis Software and Systems V, ed. G. H. Jacoby & J. Barnes (San Francisco, CA: ASP), 17

Behar, E., Sako, M., & Kahn, S. M. 2001, ApJ, 563, 497

Brown, G. V., Beiersdorfer, P., Liedahl, D. A., et al. 2002, ApJS, 140, 589

Cash, W. 1979, ApJ, 228, 939

Deslattes, R. D., Kessler, E. G., Indelicato, P., et al. 2003, RvMP, 75, 35

Drake, J. J., Ratzlaff, P., Kashyap, V., et al. 2006, Proc. SPIE, 6270, 62701I

Foreman-Mackey, D., Hogg, D. W., Lang, D., & Goodman, J. 2013, PASP, 125, 306

Foster, A. R. 2020, AN, 341, 191

Foster, A. R., & Heuer, K. 2020, Atoms, 8, 49

Fu, X.-D., Zhang, S.-N., Sun, W., Niu, S., & Ji, L. 2017, RAA, 17, 095

Gonçalves, A. C., Collin, S., Dumont, A. M., et al. 2006, A&A, 451, L23

Goodman, J., & Weare, J. 2010, CAMCS, 5, 65

Gu, L., Shah, C., Mao, J., et al. 2022, A&A, 664, A62

Hagihara, T., Yao, Y., Yamasaki, N. Y., et al. 2010, PASJ, 62, 723

Heinrich, J., & Lyons, L. 2007, ARNPS, 57, 145

Heuer, K., Foster, A. R., & Smith, R. 2021, ApJ, 908, 3

Hitomi Collaboration, Aharonian, F., Akamatsu, H., et al. 2018, PASJ, 70, 12

Houck, J. C., & Denicola, L. A. 2000, in ASP Conf. Ser. 216, Astronomical Data Analysis Software and Systems IX, ed. N. Manset, C. Veillet, & D. Crabtree (San Francisco, CA: ASP), 591

Kaastra, J. S., & Bleeker, J. A. M. 2016, A&A, 587, A151

Kaastra, J. S., Mewe, R., & Nieuwenhuijzen, H. 1996, in 11th Coll. UV And X-ray Spectroscopy Of Astrophysical And Laboratory Plasmas, ed. K. Yamashita & T. Watanabe, 411

Kallman, T., & Bautista, M. 2001, ApJS, 133, 221

Kaspi, S., Brandt, W. N., Netzer, H., et al. 2000, ApJL, 535, L17

Kaspi, S., Brandt, W. N., Netzer, H., et al. 2001, ApJ, 554, 216

Krongold, Y., Nicastro, F., Brickhouse, N. S., et al. 2003, ApJ, 597, 832

Lee, H., Kashyap, V. L., van Dyk, D. A., et al. 2011, ApJ, 731, 126

Mao, J., Mehdipour, M., Kaastra, J. S., et al. 2019, A&A, 621, A99

Mehdipour, M., Kaastra, J. S., Kriss, G. A., et al. 2017, A&A, 607, A28

Mendoza, C., Bautista, M. A., Deprince, J., et al. 2021, Atoms, 9, 12

Netzer, H., Kaspi, S., Behar, E., et al. 2003, ApJ, 599, 933

Verner, D. A., & Yakovlev, D. G. 1995, A&AS, 109, 125

Wilms, J., Allen, A., & McCray, R. 2000, ApJ, 542, 914

Xu, J., van Dyk, D. A., Kashyap, V. L., et al. 2014, ApJ, 794, 97